Inorganic Chemistry

Article

pubs.acs.org/IC

Uranium and Thorium Hydride Complexes as Multielectron Reductants: A Combined Neutron Diffraction and Quantum Chemical Study

Daniel J. Grant,[†] Timothy J. Stewart,[‡] Robert Bau,[‡] Kevin A. Miller,[§] Sax A. Mason,[⊥] Matthias Gutmann,[¶] Garry J. McIntyre,[⊥,∥] Laura Gagliardi,*[,†] and William J. Evans*[,§]

[†]Department of Chemistry, University of Minnesota and Supercomputing Institute, Minneapolis, Minnesota 55455, United States

[‡]Department of Chemistry, University of Southern California, Los Angeles, California 90089, United States

[§]Department of Chemistry, University of California at Irvine, Irvine, California 92697, United States

[⊥]Institut Laue-Langevin, BP 156, 38042 Grenoble Cedex 9, France

[¶]ISIS Facility, Rutherford Appleton Laboratory, Chilton, Didcot OX11 0QX, U.K.

Supporting Information

ABSTRACT: The unusual uranium reaction system in which uranium(4+) and uranium(3+) hydrides interconvert by formal bimetallic reductive elimination and oxidative addition reactions, $[(C_5Me_5)_2UH_2]_2$ (**1**) ⇌ $[(C_5Me_5)_2UH]_2$ (**2**) + H_2, was studied by employing multiconfigurational quantum chemical and density functional theory methods. **1** can act as a formal four-electron reductant, releasing H_2 gas as the byproduct of four H_2/H^- redox couples. The calculated structures for both reactants and products are in good agreement with the X-ray diffraction data on **2** and **1** and the neutron diffraction data on **1** obtained under H_2 pressure as part of this study. The interconversion of the uranium(4+) and uranium(3+) hydride species was calculated to be near thermoneutral (∼−2 kcal/mol). Comparison with the unknown thorium analogue, $[(C_5Me_5)_2ThH]_2$, shows that the thorium(4+) to thorium(3+) hydride interconversion reaction is endothermic by 26 kcal/mol.

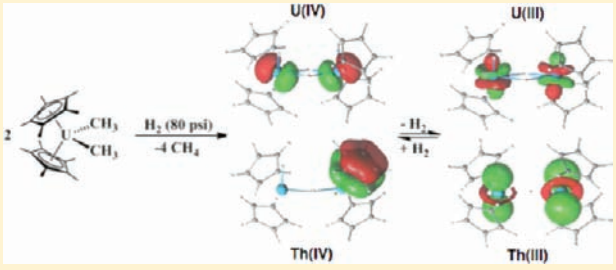

INTRODUCTION

Oxidative addition and reductive elimination reactions are rare with f elements because these metals do not have the two-electron redox couples that facilitate such reactions with transition metals. However, it has been known from the work of Marks et al. since the late 1970s that there is a facile interconversion between the dimeric uranium(4+) dihydride $[(C_5Me_5)_2UH_2]_2$ (**1**) and the dimeric uranium(3+) monohydride $[(C_5Me_5)_2UH]_2$ (**2**), as shown in eq 1 (Scheme 1).[1]

$$[(C_5Me_5)_2UH_2]_2 \rightleftharpoons [(C_5Me_5)_2UH]_2 + H_2 \quad (1)$$

Scheme 1

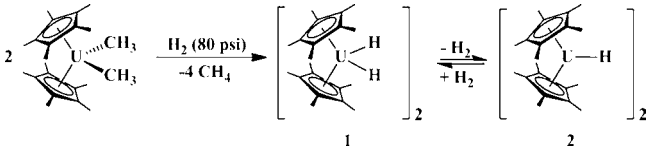

Equation 1 represents a formal bimetallic reductive elimination and oxidative addition equilibrium. For many years, this was the only example of such reactivity in f-element chemistry.

Detailed studies of the reaction system in eq 1 were hindered by the fact that neither of the hydride complexes could be isolated in pure form. However, more recent studies have led to methods to isolate both **1** and **2**, and this has allowed greater elaboration of their reaction chemistry.[2] These organoactinide hydride complexes have been found to be effective multielectron reductants in reactions in which only molecular H_2 is generated as a byproduct. Specifically, **1** and **2** cleanly reduce 2 equiv of PhEEPh (E = S, Se), 3 equiv of C_8H_8, and 2 equiv of PhN═NPh in four-, six-, and eight-electron-reduction processes, respectively (Scheme 2). The hydride complex of redox-inactive tetravalent thorium, $[(C_5Me_5)_2ThH_2]_2$ (**3**), was also shown to undergo hydride-based redox reactions with 2 and 3 equiv of PhSSPh (four-electron process) and C_8H_8 (six-electron process), respectively.[2]

Separation of **1** and **2** also allowed these molecules to be characterized by X-ray diffraction.[2] However, this provided only fingerprint information on the two complexes because the X-ray study showed only the metallocene components of the molecules; the hydrides could not be reliably located in the presence of uranium. We now report that large crystals of **1** can be

Received: November 21, 2011
Published: February 24, 2012

 © 2012 American Chemical Society dx.doi.org/10.1021/ic202503h | *Inorg. Chem.* 2012, 51, 3613−3624

Scheme 2

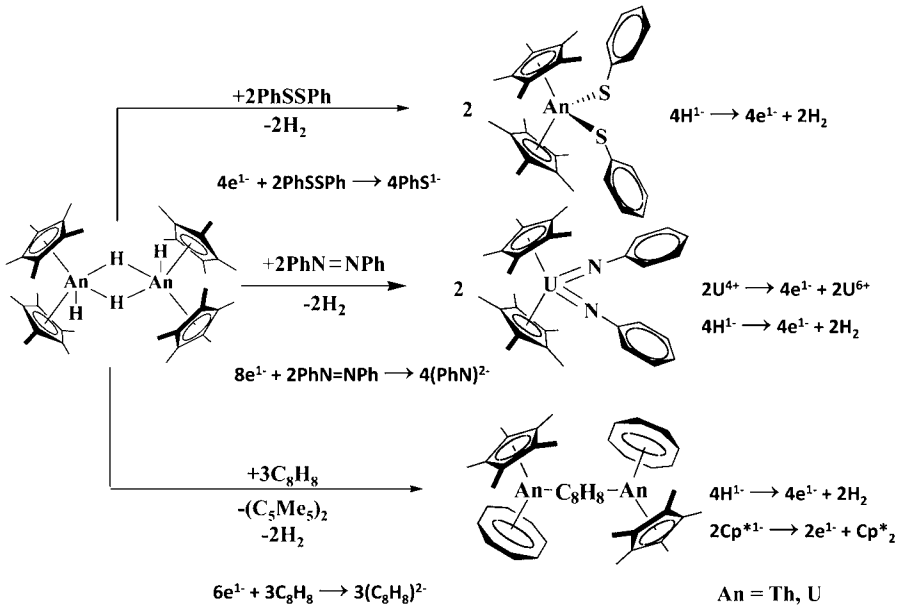

obtained under H_2 pressure. Moreover, methods were developed to seal these large crystals in capillaries under H_2, so they would last long enough to be analyzed by neutron diffraction. These data are presented here and compared with the structure of **3** previously examined by neutron diffraction by Schultz and co-workers in 1979.[3] No dimeric thorium(3+) monohydride complex, i.e., $[(C_5Me_5)_2ThH]_2$ (**4**), is known to form from **3** in analogy to eq 1. This is consistent with the dearth of molecular thorium(3+) complexes: only four examples of this unusual thorium oxidation state in organometallic complexes have been reported.[4−7]

The availability of the new neutron diffraction data on **1** meant that there was an experimental basis to which theoretical studies on both **1** and **3** can be compared. Given this opportunity and the increased reductive reactivity demonstrated for these complexes, multiconfigurational quantum chemical and density functional theory (DFT) calculations were performed on **1**−**3** and the hypothetical trivalent analogue of **2**, namely, **4**. An analysis and a comparison to available experimental data of the calculated geometries and harmonic frequencies for **1**−**4** are presented, as well as the relative energies of the possible spin states for each organoactinide hydride complex and a description of the molecular orbitals. The energetics for interconversion and the release of molecular H_2 from the tetravalent actinide hydride complexes according to eq 1 are calculated for uranium and the hypothetical thorium analogue.

EXPERIMENTAL METHODS

General Procedures. The experimental manipulations described below were performed under argon with rigorous exclusion of air and water using Schlenk, vacuum-line, and glovebox techniques. Solvents were dried over Q-5 and molecular sieves, and were saturated with argon using GlassContour columns.[8] $(C_5Me_5)_2UMe_2$ was prepared as previously described.[1] NMR spectra were recorded with a Bruker DRX 500 MHz system. IR spectra were recorded as KBr pellets on a PerkinElmer Spectrum One FT-IR spectrometer.

Crystallization of $[(C_5Me_5)_2UH(\mu\text{-}H)]_2$ (1). The addition of 4 mL of hot hexane and 4 mL of hot toluene to $(C_5Me_5)_2UMe_2$ (668 mg, 1.25 mmol) produced a saturated red solution that was transferred to a Fisher Porter high-pressure reaction vessel. This was degassed to the vapor pressure of the solvent and pressurized to 80 psi with H_2 gas. After 2 days, large black crystalline rods formed. After the pressure was reduced to 20 psi, the reaction vessel was brought into the argon glovebox, and the vessel was evacuated to the vapor pressure of the solvent and backfilled with argon three separate times. The mother liquor solvent was decanted to leave black crystals, which were analyzed by ^1H NMR and IR spectroscopy to be **1**.[1,2] X-ray samples were transferred directly from the glovebox to streaming nitrogen for diffraction sample selection.

To obtain larger (typically 4 mm^3 in size) neutron-diffraction-quality crystal samples, the reaction mixture must remain in the Fisher Porter high-pressure reaction vessel under H_2 at 80 psi for about 10 days. As long as the crystals sit in the reaction vessel at high pressure, they continue to grow, but after 10 days, many crystal samples grow on top of each other, making it difficult to separate single samples.

Because **1** converts to **2** in the absence of a H_2 atmosphere, a method for sealing the crystals under H_2 was devised (Figure 1). Crystals of **1** were mounted and flame-sealed under H_2 by the procedure described below and showed no significant decomposition for months at room temperature.

Procedure for Sealing Crystals of 1 under H_2. Figure 1 shows the apparatus used to seal **1** under H_2. A constriction was put in a 3−4-mm-i.d. quartz tube about 2.0−2.5 cm from one end. Ampules with 0.5−0.8 mm wall thickness were used to facilitate sealing. Quartz wool was inserted into the quartz tubing and packed down gently next to the constriction on the long side of the tube. In the glovebox, a crystal from a Fisher Porter pressure vessel that had just been taken

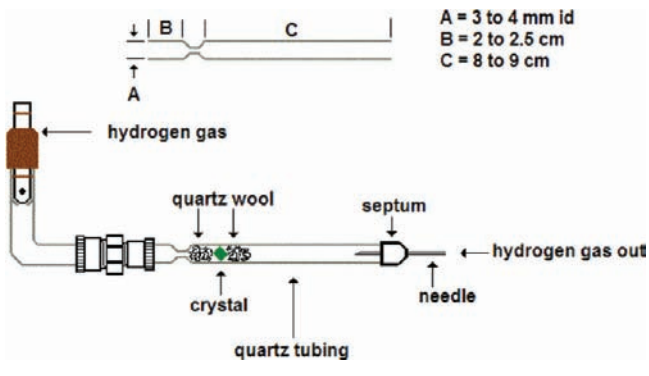

Figure 1. Method of sealing crystals of **1** under H_2. The sealing process ensured the title complex a longer shelf-life, resisting decomposition.

dx.doi.org/10.1021/ic202503h | Inorg. Chem. 2012, 51, 3613−3624

from the pressure line was inserted into the open end of the quartz tubing. Prerolled quartz wool was packed on top of the crystal. A septum was placed over the long end of the quartz tubing, and a J. Young adapter was sealed to the short end near the constriction. The apparatus was brought out of the glovebox and attached to a Schlenk line fitted with a J. Young tube fitting. The head space of the J. Young fitting was evacuated, and H_2 gas was introduced into the system by opening the J. Young adapter. A needle was inserted in the septum, and the H_2 gas that exited was lit with a flame. The large end of the quartz tubing was sealed with a torch, and then the constricted end of the quartz tubing was quickly sealed with a torch.

Neutron Data Collection, Structure Determination, and Refinement of 1. Neutron diffraction data were collected at 33 K on SXD, the single crystal diffractometer at the ISIS spallation neutron source.[9] The ampule was mounted in an aluminum block and shielded with cadmium to minimize background scattering from the aluminum. Each crystal orientation was exposed to the neutron beam for 2.5 h per orientation at positions of $\omega = -90°$, $-150°$, $-40°$, $0°$, and $+90°$ (five orientations). The crystal was then tilted by 45° in χ, and four more orientations were collected, $\omega = +90°$, $+150°$, $+130°$, and $0°$, yielding a total of 11 sets of data, with each set consisting of the results from 11 detectors. Data reduction, integration, and absorption correction were performed using the *SXD2001* software. The intensities were extracted using a least-squares procedure with a three-dimensional Gaussian ellipsoid, taking into account the asymmetry with respect to time-of-flight as a profile function. For the absorption correction, the following expression was used: $\mu = 3.1447 + 0.0063*\lambda$ (λ = wavelength in Å; μ in cm^{-1}). The minimum, maximum, and average transmissions were 1.618, 2.262, and 1.715, respectively. The minimum *d*-spacing is equal to 0.31 Å, and the wavelength ranged from 0.37 to 8.8 Å. The minimum and maximum 2θ values were 12.5 and 165°, respectively. As part of the time-sorted Laue procedure, the wavelength and 2θ ranges are combined (i.e., at each 2θ value), and the full wavelength range is recorded.

Initial X-ray atomic coordinates obtained at the University of Southern California, as described in the Supporting Information of the primary uranium and carbon framework, were used to phase the neutron data. The final refinement of the structural analysis gives an agreement factor of 17.9% for 2478 unique reflections, R1 = 16.7%, wR2 = 43.4%, for those data with $I > 2\sigma(I)$, and all atoms refined anisotropically. The total data-to-parameter ratio was 15:1, and the goodness of fit on F^2 equals 1.00. *Z* equals 8, and unit cell dimensions were a = 18.943(4) Å, b = 12.818(3) Å, c = 16.129(4) Å, and β = 104.742(15)°. Relevant crystallographic data are summarized in Table 1.

The 33 K collection temperature was attempted to improve disorder in the $(C_5Me_5)^-$ rings. However, the cooler temperature did not improve $(C_5Me_5)^-$ ring disorder. An obvious case of position disorder in the $(C_5Me_5)^-$ ring ligands was located in the cyclopentadienyl flat plane. A second set of ring-atom positions was located and included in the model. The sum of the variable occupancy factors for the two possible ring configurations was constrained to be 1.0. For clearer imaging, geometrical restraints were applied to obtain target bond lengths and angles (1.34 Å sp^2 C−C and 120° C1−C3). Also appearing are different nuclear configurations where the methyl substituent group bond angles approach 110 and 125° in alternating pairs instead of all bond angles of 120°. Therefore, the methyl substituents were restrained to target 1.54 Å bond lengths and 120° angles.

A second, better neutron diffraction data set was collected at 208 K on a single crystal of approximate volume 23 mm^3 using the D19 diffractometer at the Institut Laue-Langevin (ILL) in Grenoble, France. The sample was presealed in a quartz tube, which was mounted on a Displex cryorefrigerator on the ILL thermal-beam diffractometer D19 equipped with a new large horizontally curved position-sensitive detector.[10] This detector is mounted symmetrically about the equatorial plane with sample-to-detector distance of 76 cm and subtends 30° vertically and 120° horizontally. It is based on a novel multiwire gas counter technology with a readout of 256 × 640 pixels/frame with pixel spacings 0.12° vertically and 0.19° horizontally. The chosen neutron wavelength was 1.4587(1)Å from a Cu(220) monochromator in reflection, take-off angle 70°. The crystal was cooled slowly to 208 K (3 K/min), while the diffraction pattern was monitored, and during cooling, some very weak superlattice reflections appeared at about 217 K, suggesting possible tripling of *b*. However, at 208 K, the average space group and the unit cell found by X-ray diffraction were used for refinement. The accessible reflections up to 2θ = ∼122° were measured, to preset monitor counts, in a series of 80° ω scans typically in steps of 0.07° and counting times of about 4 s/step. The average number of reflections per detector frame (i.e., at any one orientation) was 42.

A range of crystal orientations (different φ and χ positions) were used to explore as much of the reciprocal space as time permitted. Because of its large horizontal opening, only one detector position was required. Between the long 1.5 h scans, three strong reflections were monitored in a single short scan and showed no significant change. The total measurement time at 208 K was almost 1 day.

Raw intensity data were corrected for vertical and horizontal positional distortion. Bragg intensities were integrated in three dimensions using a version of the ILL program *Retreat*,[11] which was modified for the new detector geometry. The unit cell dimensions were calculated (ILL program Rafd19) at the end of the integration from the centroids of 2233 strong reflections ($6.0 < 2\theta < 121.9°$); the mean positional errors for the centroids were 0.02, 0.03, and 0.11° in the scan, horizontal, and vertical directions respectively.

A total of 7793 Bragg reflections were obtained, of which 3228 were independent with $-22 \le h \le 17$, $-15 \le k \le 9$, and $-19 \le l \le 18$. The Bragg intensities were corrected for attenuation by the cylindrical aluminum and vanadium Displex heat shields (minimum and maximum transmission coefficients 0.8003 and 0.8958) using the ILL program *Abscan*. Data collection parameters are given in Table 1.

X-ray atomic coordinates as described above of the primary uranium and carbon framework were used to phase the 208 K neutron data. *SHELXL* residual values for **1** at convergence are R1 = 0.114 and

Table 1. Crystallographic Data Collection Parameters for 1

	$C_{40}H_{64}U_2$	$C_{40}H_{64}U_2$	$C_{40}H_{64}U_2$	$C_{40}H_{64}U_2$
facility	UCSD[2]	USC	ISIS	ILL
source	Mo X-ray	Mo X-ray	spallation	reactor
fw	1020.99	1016.94	1021.00	1021.00
temp (K)	208(2)	148(2)	33(2)	208(1)
λ (Å)	0.710 73	0.710 73	0.37−8.80	1.4587(1)
cryst syst	monoclinic	monoclinic	monoclinic	monoclinic
space group	*C*2/*c*	*C*2/*c*	*C*2/*c*	*C*2/*c*
a (Å)	18.8970(1)	18.968(3)	18.943(4)	18.879(1)
b (Å)	12.8770(7)	12.864(2)	12.818(3)	12.882(1)
c (Å)	16.2190(9)	16.141(3)	16.129(4)	16.229(3)
α (deg)	90.000	90.000	90.000	90.000
β (deg)	104.811(1)	104.680(2)	104.742(15)	104.909(5)
γ (deg)	90.000	90.000	90.000	90.000
cryst size (mm^3)	0.0017	0.1750	4	23
V ($Å^3$)	3815.5(4)	3809.7(11)	3787.3(14)	3814.0(3)
Z	8	8	8	8
GOF	1.103	1.039	1.002	1.036
no. of reflns	13 055	11 069	8838	7793
no. of indep reflns	4442	4231	2478	3228
ρ_{calcd} (Mg/m^3)	1.774	1.773	1.791	1.780
μ (mm^{-1})	8.502	8.515	see text	
R1 [$I > 2.0\sigma(I)$][a]	0.0477	0.0549	0.1668	0.1142
wR2 (all data)[a]	0.1225	0.1498	0.4344	0.2597

[a] $R1 = \sum||F_o| - |F_c||/\sum|F_o|$. $wR2 = [\sum[w(F_o^2 - F_c^2)^2]\sum[w(F_o^2)^2]]^{1/2}$.

dx.doi.org/10.1021/ic202503h | *Inorg. Chem.* 2012, 51, 3613−3624

wR2 = 0.2403, for those data with $I > 2\sigma(I)$. The data-to-parameter ratio is 5:1, and the goodness of fit on F^2 equals 1.036. Z equals 8, and unit cell dimensions were a = 18.879(1) Å, b = 12.882(1) Å, c = 16.229(1) Å, and β = 104.909(5)°. Relevant crystallographic data are summarized in Table 2. Full crystallographic data are listed in the Supporting Information.

Table 2. Selected Bond Distances (Å) and Angles (deg) for $[(C_5Me_5)_2UH(\mu\text{-}H)]_2$

	$C_{40}H_{64}U_2$	$C_{40}H_{64}U_2$	$C_{40}H_{64}U_2$	$C_{40}H_{64}U_2$
facility	UCSD/UCI[2]	USC	ISIS	ILL
source	Mo X-ray	Mo X-ray	spallation	reactor
U1−U1A	3.606(6)	3.689(1)	3.684	3.604
U1−Cnt1	2.499	2.494	2.491	2.547
U1−Cnt2	2.475	2.487	2.479	2.459
U1−C1	2.801(9)	2.743(9)	2.746(6)	2.719(11)
U1−C2	2.768(9)	2.745(9)	2.737(5)	2.732(10)
U1−C3	2.725(9)	2.804(9)	2.780(5)	2.786(10)
U1−C4	2.740(8)	2.773(9)	2.775(10)	2.751(10)
U1−C5	2.750(9)	2.728(9)	2.733(6)	2.695(11)
U1−C11A	2.867(6)	2.736(12)	2.779(6)	2.830(13)
U1−C12A	2.809(7)	2.717(15)	2.765(6)	2.783(10)
U1−C13A	2.794(7)	2.726(14)	2.769(7)	2.801(11)
U1−C14A	2.843(7)	2.747(10)	2.733(10)	2.813(13)
U1−C15A	2.888(6)	2.735(12)	2.753(7)	2.840(13)
U1−C11B	2.755(6)	n/a	2.747(26)	2.703(17)
U1−C12B	2.754(7)	n/a	2.772(17)	2.678(14)
U1−C13B	2.738(7)	n/a	2.802(25)	2.674(15)
U1−C14B	2.729(6)	n/a	2.676(19)	2.680(20)
U1−C15B	2.739(7)	n/a	2.867(22)	2.691(14)
U1−H1U (bridge)	1.94(9)	n/a	2.201(17)	2.148(7)
U1−H1UA (bridge)	n/a	n/a	2.135(9)	2.134(9)
U1−H3 (terminal)	n/a	n/a	2.006(21)	2.052(15)
Cnt1−U1−Cnt2	127.6	128.86	128.64	126.75
Cnt1−U1−H1U	115.3	n/a	117.99	117.51
Cnt1−U1−H1UA	92.6	n/a	88.36	89.47
Cnt2−U1−H1U	101.0	n/a	99.20	98.00
Cnt2−U1−H1UA	139.5	n/a	142.96	142.38
Cnt1−U1−H3	n/a	n/a	95.40	94.37
Cnt2−U1−H3	n/a	n/a	91.07	92.28

Computational Methods. Quantum chemical calculations were performed using DFT[12,13] and multiconfigurational methods followed by second-order perturbation theory (CASSCF/CASPT2).[14,15] The starting structures for geometry optimizations were taken from the available experimental crystal structures of $[(C_5Me_5)_2UH_2]_2$ (**1**),[2] $[(C_5Me_5)_2UH]_2$ (**2**),[2] and $[(C_5Me_5)_2ThH_2]_2$ (**3**).[3] Given the absence of a crystal structure for **4**, its starting structure was approximated by removal of the terminal hydrides of **3**.

Geometry optimizations were performed at the DFT level with the Perdew−Burke−Ernzerhof (PBE) exchange-correlation functional[16] and a triple-ζ valence plus polarization (def-TZVP)[17] basis set on all atoms. Quasi-relativistic pseudopotentials were used for the Th and U atoms with a core of 60 electrons.[17,18] Single-point calculations for the various possible spin states were performed at the respective starting structures at the PBE/def-TZVP level. Geometry optimizations were performed solely for the lowest spin states. Vibrational harmonic frequencies were calculated analytically to ensure that the optimized structures are indeed minima that are not characterized by any imaginary frequencies. The zero-point energies were included in the calculation of the interconversion energies. All DFT calculations were performed with the *TURBOMOLE 5.10* program package.[17,19]

Single-point multiconfigurational complete active space (CASSCF)[14] calculations followed by second-order perturbation theory (CASPT2)[15] were performed at the DFT-optimized (PBE/def-TZVP) geometries. Scalar relativistic effects were included using the Douglas−Kroll−Hess[20] Hamiltonian to second order and the relativistic all-electron ANO-RCC basis sets with double-ζ quality (ANO-RCC-VDZP)[21] with the following contractions: [8s7p5d3f1g] for the Th and U atoms and [3s2p1d] for the C atom. The ANO-RCC-MB basis set was employed for the H atom with a contraction of [1s]. In order for the CASPT2 calculations to be computationally feasible, the methyl groups of the pentamethylcyclopentadienyl ligands were replaced with H atoms. The CASPT2 calculations for the possible spin states of the tetravalent and trivalent uranium complexes were performed at the quintet and septet DFT-optimized geometries, respectively. For the trivalent thorium hydride complex, the CASPT2 calculations of the triplet and singlet states were performed at their respective DFT-optimized geometries. Several active spaces were initially tested, and the final active space for the tetravalent uranium and thorium hydride complexes included 12 electrons in 12 orbitals. For the trivalent analogues, the final active space included 14 electrons in 14 orbitals. For the thorium hydride complexes, the orbitals mainly include the bonding and antibonding orbitals between C atoms of the cyclopentadientyl ligands, in contrast to those of the uranium hydride complexes that were found to be the 6p and 5f orbitals localized on uranium.

The CASPT2 calculations were performed with the *MOLCAS 7.3* package.[22] The computational costs arising from the two-electron integrals were drastically reduced by employing the Cholesky decomposition technique in all CASPT2 calculations[23−25] combined with the local exchange screening.[26] The CASPT2 approach has been successful in the study of many actinide-containing systems.[27−30]

RESULTS

X-ray and Neutron Diffraction. The solid-state structure of **1** was initially determined by single-crystal X-ray diffraction analysis at 208 K.[2] Repeated attempts to obtain low-temperature (150 K) X-ray diffraction data were unsuccessful because the crystals cracked during data collection. At room temperature, the crystal showed no sign of cracking in the paratone oil used to mount the crystals in a nylon loop.

To gain better low-temperature X-ray diffraction data on the non-H atoms to be used to evaluate the neutron data that would be collected at low temperature, crystals of **1** were "snap-frozen" by selecting the single-crystal sample under streaming nitrogen gas and transferring it with cryotongs to the goniometer head, where there was streaming nitrogen gas. This allowed X-ray data to be collected at 148(2) K. Both X-ray experiments showed that the space group for **1** was $C2/c$ (Table 1). There is one crystallographically independent molecule in the unit cell, and the metallocenes are equivalent by symmetry.

Complex **1** was analyzed by neutron diffraction at both 33 and 208 K. The X-ray atomic coordinates were used to phase the neutron residual data, and the final arrangement of the heavy atoms was found to be the same as that determined by X-ray diffraction (Figure 2). Table 2 shows a comparison of the bond distances and angles in the four structure determinations. Variations in the data are present, in part, because of the different data collection temperatures. Hence, the 3.606(6) and 3.604 Å U···U distances for the X-ray data at 208(2) K and the neutron data at 208(1) K are identical but differ from the 3.689(1) and 3.684 Å analogues in the X-ray data at 148(2) K and the neutron data at 33(2) K. The data from the ILL experiment will be used primarily in the comparisons because all of the R values are lower than those in the ISIS experiment.

dx.doi.org/10.1021/ic202503h | *Inorg. Chem.* 2012, 51, 3613−3624

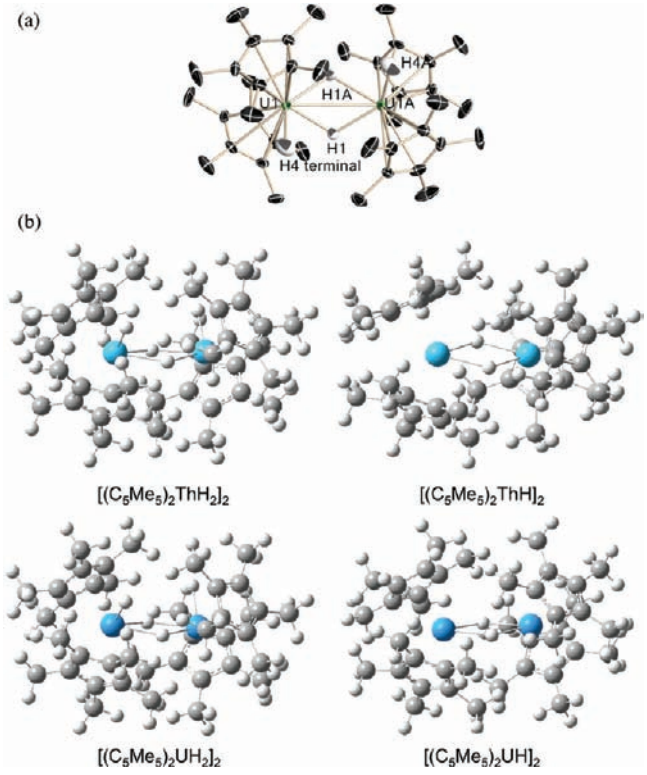

Figure 2. (a) Thermal ellipsoid plot of **1** drawn at the 50% level from neutron data at 208 K. (b) Optimized molecular structures of $[(C_5Me_5)_2AnH_2]_2$ and $[(C_5Me_5)_2AnH]_2$ (An = Th, U) at the PBE/def-TZVP level. Color code: Th and U, blue; C, gray; H, white.

The neutron experiments allowed the hydride ligands to be located. A terminal hydride was found on each of the symmetric metallocene units. Two hydrides bridging uranium were also located and refined anisotropically. However, neutron data sets indicated an additional bridging hydride atom disordered about a special position. The appearance of three bridging hydrides was assumed to arise from the presence of one regular bridging hydride (i.e., one hydride has a sof equaling 1.0) and one that is disordered between two positions (i.e., two hydrides have sof's equaling 0.5 each). Two possibilities to eliminate the geometrical problem were explored. First, the *C*2/*c* space group was changed to a lower *Cc* space group, which eliminates the 2-fold symmetry axis with this particular special position. However, three hydride positions were once again located. Second, disorder was assumed about this third particular special position, and the sof's of all three bridging hydrides were allowed to refine independently of the rest of the molecules. On the basis of the refined sof, the three separate positions were discovered to sum to a total two hydrides occupancy. This result is consistent with the previously published X-ray data that allowed the bridging hydrides to be located on a difference map. The special position hydride has a U1−H1 bond distance of 2.148(7) Å.

Theoretical Studies. The relative energies of the possible spin states, highest occupied molecular orbital (HOMO)−lowest unoccupied molecular orbital (LUMO) gaps, and S^2 values are reported in Table 3. Selected optimized geometry parameters for **1**−**4** are reported in Tables 4−7 and compared to experimental crystallographic data. The optimized molecular structures are illustrated in Figure 2 and provided as xyz coordinates in the Supporting Information. The calculated and experimental harmonic stretching frequencies between the actinide metal and the terminal and bridging hydrides are reported in Table 8. The molecular orbital plots responsible for bonding in the HOMO−LUMO region are presented in Figures 3−6. The molecular orbitals indicating bonding between the actinide metal and bridging hydrides are presented in Figure 7. In the following, we will first discuss the relative energies and then structural parameters and frequencies.

Relative Energies. The tetravalent thorium hydride complex **3** with a $5f^0$ thorium configuration is predicted to have a closed-shell singlet ground state. For the trivalent thorium complex **4** with a $6d^1$ electron configuration on each thorium, two spin states are possible, with the triplet state lying 22.1 kcal/mol lower based on single-point calculations at the PBE/def-TZVP level at the geometry initially used to approximate the structure. Upon geometry optimization, this energy difference decreased to 8.3 kcal/mol (Table 3). In addition, CASPT2/ANO-RCC-VDZP calculations indicated the triplet state to be the ground state by 6.6 kcal/mol. The CASPT2 and PBE methods agree to within 2 kcal/mol in predicting the relative state energies of **4**.

The analogous tetravalent and trivalent uranium hydride complexes are slightly more complicated by the existence of several spin states that arise from coupling of the U $5f^2$ and $5f^3$ electrons, respectively. At the PBE level, tetravalent **1** is predicted to have a quintet ground state, with triplet and singlet states lying 17.7 and 38.5 kcal/mol higher in energy, respectively. The quintet and singlet states are pure spin states with S^2 values of 3.0 and 0.0, respectively; however, the triplet state is characterized by substantial spin contamination [S^2 value of 3.0 (Table 3)]. At the CASPT2 level, the triplet and singlet states are actually predicted to be 0.3 and 0.4 kcal/mol below the quintet state, respectively, indicating a reversal of the relative

Table 3. Relative Energies Calculated at the CASPT2 and PBE Levels (kcal/mol), HOMO−LUMO Gap (eV), and S^2 Values

		CASPT2/ANO-RCC-VDZP				PBE/def-TZVP	
molecule	state	(12, 12)	(14, 14)	PBE/def-TZVP	PBE/def-SVP	HOMO−LUMO	S^2
$[(C_5Me_5)_2ThH_2]_2$	singlet					2.699	0.00
$[(C_5Me_5)_2ThH]_2$	triplet		0.0	0.0	0.0	0.532	2.00
	singlet		6.6	8.3	8.8		0.00
$[(C_5Me_5)_2UH_2]_2$	quintet	0.0		0.0	0.0	2.434	6.04
	triplet	−0.3		17.7	6.5		3.01
	singlet	−0.4		38.5	36.2		0.00
$[(C_5Me_5)_2UH]_2$	septet		0.0	0.0	0.0	2.888	12.02
	quintet		−0.2	13.8	14.1		7.00
	triplet		−0.5	12.3	12.6		3.99
	singlet		−0.8				

dx.doi.org/10.1021/ic202503h | *Inorg. Chem.* 2012, 51, 3613−3624

Table 4. Selected Geometry Parameters of 3 Calculated at the PBE Level[a]

state	basis set	r(Th−Th)	r(Th−H)	r(Th−C)	r(C_r−C_r)	r(C_r−C_{me})	r(C−H)	∠Cp−Th−Cp
singlet	def-SVP	4.001	2.091_t, $2.268–2.298_b$	2.81−2.86	1.431−1.439	1.503−1.507	1.109−1.118	132
	def-TZVP	4.002	$2.081–2.082_t$, $2.273–2.296_b$	2.813−2.867	1.426−1.434	1.500−1.503	1.097−1.105	131
	expt[b]	*4.007(8)*	*$2.03(1)_t$, $2.29(3)_b$*	*2.83(1)*	*1.43(1)*	*1.50(1)*	*1.05(1)*	*130(1)*

[a]Experimental data from the crystal structure are given in italics. Distances are in Å and angles in deg. When two values are given, the range represents the shortest and longest, respectively. Notations: r = ring, me = methyl, t = terminal, b = bridge, and Cp = pentamethylcyclopentadienyl. [b]Reference 2.

Table 5. Selected Geometry Parameters of 4 Calculated at the PBE Level[a]

state	basis set	r(Th−Th)	r(Th−H)$_b$	r(Th−C)	r(C_r−C_r)	r(C_r−C_{me})	r(C−H)	∠Cp−Th−Cp
triplet	def-SVP	4.003	2.289−2.294	2.772−2.853	1.432−1.442	1.503−1.508	1.108−1.118	131
	def-TZVP	4.001	2.285−2.291	2.786−2.858	1.426−1.436	1.499−1.504	1.096−1.106	131
singlet	def-SVP	3.893	2.245−2.263	2.740−2.845	1.427−1.446	1.499−1.508	1.108−1.118	130
	def-TZVP	3.851	2.233−2.259	2.770−2.862	1.423−1.436	1.498−1.504	1.096−1.109	130

[a]Distances are in Å and angles in deg. When two values are given, the range represents the shortest and longest, respectively. Notations: r = ring, me = methyl, b = bridge, and Cp = pentamethylcyclopentadienyl.

energies of the spin states. The PBE value differs by as much as 39 kcal/mol compared to the CASPT2 value. At the PBE level, trivalent **2** is predicted to have a septet ground state, with the quintet and triplet states lying 13.8 and 12.3 kcal/mol higher in energy, respectively. Similarly, both quintet and triplet states are characterized by substantial spin contamination with S^2 values of 7.0 and 4.0, respectively (Table 3). As seen in **1**, the CASPT2 calculation predicts a different ground state compared to the PBE result, with the quintet, triplet, and singlet states predicted to be 0.2, 0.5, and 0.8 kcal/mol below the septet state. Compared to the CASPT2 value, the PBE value differs by as much as 14 kcal/mol because of spin contamination. In the prediction of the relative state energies of actinide hydrides, DFT is less reliable because of the presence of substantial spin contamination; however, both CASPT2 and DFT are in excellent agreement when spin contamination is absent, as seen in the trivalent thorium analogue **3**.

Geometries and Frequencies. The geometrical parameters calculated at the PBE/def-TZVP and PBE/def-SVP levels are in good agreement with the experimental crystallographic data for **1**−**3**,[2,3] and unless specified, the def-TZVP values are discussed below. Closed-shell **3** will be discussed first (Table 4). The calculated r(Th−Th) bond distances of 4.001 and 4.002 Å are very close to the experimental value of 4.007(8) Å.[2,3] It has previously been noted that the latter value seems large compared to the 3.632(2) Å Th···Th distance in $\{[Me_2Si(C_5Me_4)_2]ThH_2\}_2$.[31] The calculated r(Th−H) terminal bond distance was 0.05 Å longer than the experimental value, while the calculated r(Th−H) bridging bond distance was essentially the same as the experimental value when considering the error bar limits.[2,3] The range of values calculated for the r(Th−C) (carbon of the pentamethylcyclopendienyl ligand) bond distance bracketed the experimental value of 2.83(1) Å.[2,3] Excellent agreement was also found for other selected bond distances, specifically r(C_{ring}−C_{ring}), r(C_{ring}−C_{me}), and r(C−H). The (C_5Me_5 ring)−Th−(C_5Me_5 ring) angle was found to be 131°, in excellent agreement with the crystal structure value of 130(1)°.[2,3] A rather interesting feature of the calculation is the prediction of a nonplanar $Th_2(\mu\text{-}H)_2$ unit in contrast to the neutron data: the dihedral angle ∠Th−H_2−Th is predicted to be 169.9°. The calculated ∠H−Th−H and ∠Th−H−Th angles of 56.8 and 122.4° are in excellent agreement with the experimental values of 58(1) and 122(4)°, respectively, considering the error bars.

Because the trivalent **4** (Table 5) is unknown, the calculated structure will be compared to the experimental structure of its tetravalent thorium analogue, **3**, and that of the trivalent uranium complex **2**. The calculation predicts a symmetrical dimeric structure with both hydrides in bridging positions. The calculated r(Th−Th) bond distances of the triplet and singlet structures of **4** are 0.006 and 0.156 Å shorter than the experimental distance in **3**, respectively. This is unusual because the radius of Th^{3+} is expected to be larger than Th^{4+} given that the An^{3+} radii for An = U, Np, and Pu are found to be 0.14 Å larger than the An^{4+} radii.[32] Larger distances would also be expected in **4** because the 3.8651(7) and 3.8530(7) Å U···U distances in trivalent **2** are larger than the 3.603−3.689 Å U···U distances in tetravalent **1**.[2] No theoretical evidence was found to suggest that the two $6d^1$ ions in **4** were forming a metal−metal interaction that could lead to the shorter Th···Th distance. The (C_5Me_5 ring)−Th−(C_5Me_5 ring) angle in **4** was calculated to be 131°, similar to the 130(1)° value in **3**, the 128.5−133.8° values in **2**, and the 126.8−128.9° angle in **1**. In contrast to **3**, the $Th_2(\mu\text{-}H)_2$ unit is planar in both the triplet (∠Th−H_2−Th angle of 179.4°) and open-shell singlet (∠Th−H_2−Th angle of 179.2°) structures.

For **1**, the geometry parameters for both the quintet and triplet states were calculated. However, the spin contamination of the triplet state was significant with an S^2 value of 3.0 instead of 2.0 (Table 3), indicating that the converged triplet calculation did not correspond to a pure triplet spin state but rather to a mixture of triplet and quintet states. Only the values for the pure quintet state will be discussed. The calculated r(U−U) bond distances, 3.868−3.872 Å, are significantly longer than the 3.604−3.689 Å distances found by X-ray and neutron diffraction. As noted above, this range of experimental values is likely due to the difference in data collection temperatures. The calculated r(U−H) terminal and bridging bond distances are much closer to the experimental values: terminal, 2.014−2.020 Å calcd and 2.01(2)−2.05(2) Å expt; bridging, 2.196−2.206 Å calcd and 2.13(1)−2.20(2) Å expt. This contrasts with the calculation on **3** that gave closer Th−Th than Th−H distances. The remaining selected bond distances (Table 6) were in excellent agreement with the experimental values[2] to within 0.01 Å. The (C_5Me_5 ring)−U−(C_5Me_5 ring) angle was

dx.doi.org/10.1021/ic202503h | Inorg. Chem. 2012, 51, 3613−3624

Table 6. Selected Geometry Parameters of 1 Calculated at the PBE Level[a]

state	basis set	r(U−U)	r(U−H)	r(U−C)	r(C$_r$−C$_t$)	r(C$_r$−C$_{me}$)	r(C−H)	∠Cp−U−Cp
quintet	def-SVP	3.868	2.014$_t$, 2.196−2.206$_b$	2.694−2.818	1.431−1.439	1.502−1.507	1.108−1.118	129
	def-TZVP	3.872	2.020$_t$, 2.195−2.203$_b$	2.713−2.830	1.424−1.433	1.498−1.503	1.096−1.105	129
triplet	def-SVP	3.895	2.016−2.020$_t$, 2.199−2.221$_b$	2.684−2.8209	1.430−1.440	1.503−1.508	1.107−1.118	129
	def-TZVP	3.827	2.017$_t$, 2.181−2.187$_b$	2.730−2.822	1.425−1.433	1.498−1.504	1.096−1.105	129
	expt[b,c]	*3.604−3.689(1)*	*2.01(2)−2.05(2)$_t$, 2.13(1)−2.20(2)$_b$*	*2.676(19)−2.888(6)*	*1.44(1)*	*1.50(1)*	*1.10−1.11*	*126.8−128.9*

[a]Experimental data from the crystal structure are given in italics. Distances are in Å and angles in deg. When two values are given, the range represents the shortest and longest, respectively. Notations: r = ring, me = methyl, t = terminal, b = bridge, and Cp = pentamethylcyclopentadienyl. [b]Reference 2. [c]This work.

129° in all four calculations and close to the 126.8−128.9° range of the experimental values. The ∠U−H$_2$−U angle was predicted to be 172.7°, in excellent agreement with the experimental value[2] of 172.5°.

For **2**, the structures of both the septet and quintet states were comparable to the crystallographic structure. However, the quintet state was characterized by large spin contamination, and the values discussed below are for the septet structure, which is a pure spin state (S^2 value of 12.0; Table 3). The 3.878−3.891 Å calculated *r*(U−U) bond distances are very close to the 3.8530(7) and 3.8651(7) Å observed values. In contrast to the thorium complexes **3** and **4**, the calculations for the uranium complexes **1** and **2** give longer bond distances for the trivalent metal, as is expected and experimentally observed. Because the *r*(U−H) bridging bond distance was not observed experimentally, direct comparisons cannot be made. However, the 2.252−2.256 Å *r*(U−H) bridging bond distances calculated for **2** are longer than the calculated (2.195−2.203 Å) and experimental [2.13(1)−2.20(2) Å] values for **1**, as is expected for a trivalent ion with a larger radius. The 130° (C_5Me_5 ring)−U−(C_5Me_5 ring) angle for **2** is in the middle of the range of experimental values, 128.5−133.8°. The calculated ∠U−H$_2$−U angle was predicted to be 176.0°, showing a slight increase in planarity compared to that of **1**. Irrespective of the actinide metal, the ∠An−H$_2$−An (An = Th, U) angle varies by a mere 10° and is planar compared to a butterfly structure. The remaining geometry parameters similarly show good agreement with the experimental values.[2]

Harmonic frequencies have been calculated at the PBE/def-TZVP level, and each molecule is characterized by a small imaginary frequency of less than 25 cm^{-1} [(**1**, quintet), 14.9*i* cm^{-1}; (**2**, septet), 8.6*i* cm^{-1}; (**3**, singlet), 19.3*i* cm^{-1}; (**4**, triplet), 22.2*i* cm^{-1}] possibly because of the use of a relatively loose grid upon optimization. The calculated symmetric and asymmetric stretches between the actinide metal and terminal or bridging hydrides are listed in Table 8 and compared to the experimental values. The calculated values are 75 cm^{-1} higher than the maximum of the experimentally observed absorptions, but these bands are quite broad. The bridging An−H stretching frequencies for uranium are slightly lower than those of thorium, whereas the reverse is found for the terminal An−H stretches.

Natural Orbitals. The natural orbitals along with their occupation numbers obtained at the CASPT2/ANO-RCC-VDZP level are plotted in Figures 3−6. For **3**, the natural orbitals are largely localized on the cyclopentadienyl ligands and correspond to bonding and antibonding orbitals (Figure 3). In addition, there is a delocalized orbital just below the HOMO−LUMO region, showing some bonding between thorium and the bridging hydrides, as well as some bonding between C atoms of the cyclopentadienyl ligands (Figure 7). As is expected for a closed-shell singlet molecule, the wave function of **3** is largely a single electronic configuration, $6\pi_{(C-C)_{Cp}*}{}^2$, with a weighting of 0.88.

The natural orbitals of trivalent **4** (Figure 4) were rather similar to those of the tetravalent analogue **3**, being largely localized on the cyclopentadienyl ligands, except for two orbitals, which corresponded to the unpaired electrons on thorium. The orbitals with an occupation of 1.00 had significant amounts of s and d character only and essentially correspond to a 6d^1 electron configuration, consistent with the experimentally determined electron configuration for Th^{3+} in known complexes.[4−7] A natural orbital also lies just below the HOMO−LUMO re-

dx.doi.org/10.1021/ic202503h | Inorg. Chem. 2012, 51, 3613−3624

Table 7. Selected Geometry Parameters of 2 Calculated at the PBE Level[a]

state	basis set	r(U−U)	r(U−H)$_b$	r(U−C)	r(C$_r$−C$_r$)	r(C$_r$−C$_{me}$)	r(C−H)	∠Cp−U−Cp
septet	def-SVP	3.891	2.256−2.258	2.719−2.812	1.431−1.440	1.504−1.509	1.109−1.118	130
	def-TZVP	3.878	2.252−2.256	2.731−2.824	1.425−1.435	1.500−1.505	1.096−1.105	130
quintet	def-SVP	3.912	2.227−2.277	2.705−2.801	1.432−1.442	1.504−1.509	1.108−1.118	130
	def-TZVP	3.894	2.240−2.273	2.718−2.806	1.426−1.437	1.500−1.505	1.096−1.106	131
	expt[b,c]	*3.853−3.865*	*2.13(1)−2.20(2)*	*2.72−2.81*	*1.37−1.44*	*1.48−1.52*	*0.98*	*128.5−133.8*

[a]Experimental data from the crystal structure is given in italics. Distances are in Å and angles in deg. When two values are given, the range respresents the shortest and longest, respectively. Notations: r = ring, me = methyl, b = bridge, and Cp = pentamethylcyclopentadienyl. [b]Reference 2. [c]The bridging H atoms were not identifiable in the crystal structure, and the values given in the table correspond to those in **1**.

Table 8. Calculated Harmonic Symmetric and Asymmetric Stretching Frequencies of the Bridging and Terminal Hydrides at the PBE/def-TZVP Level (cm^{-1})[a]

		PBE/def-TZVP	
molecule	state	terminal	bridging
$[(C_5Me_5)_2ThH_2]_2$	singlet	1398.7/1399.7	1233.41/1162.5
	expt	*1404/1370*	*1215/1115*
$[(C_5Me_5)_2ThH]_2$	triplet		1208.1/1128.2
$[(C_5Me_5)_2UH_2]_2$	quintet	1414.3/1408.8	1192.6/1179.4
	expt	*1335*	*1180*
$[(C_5Me_5)_2UH_2]_2$	septet		1129.8/1118.0

[a]The first value given is for the symmetric stretch, and the second value is for the asymmetric stretch. Experimental values are given in italics.[2]

gion, showing bonding between thorium and the bridging hydrides; however, the electron density of this actinide−hydride bond shows less delocalization compared to that of **3** (Figure 7). Similarly, as found for **3**, **4** is largely dominated by a single electronic configuration of $6\pi_{(C-C)_{Cp}*}{}^2$ 2Th $6d^1$ with a weight of 0.91.

The natural orbitals of tetravalent **1** are essentially localized on uranium as opposed to the cyclopentadienyl ligands in **3** and **4** (Figure 5). The orbitals with an occupation of ∼1.99 correspond to U 6p orbitals, while those with an occupation of 1.00 correspond to U 5f orbitals. Similarly, a delocalized orbital lies just below the HOMO−LUMO region and shows a bonding interaction between uranium and the bridging hydrides, as well as between C atoms of the cyclopentadienyl ligands (Figure 7). A wave-function analysis of **1** indicates a dominant single electronic configuration of 4U $6p^2$ 2U $5f^2$ with a weight of 0.98.

The natural orbitals of the trivalent uranium analogue **2** (Figure 6) are similar to those of its tetravalent counterpart, showing localization of the U 6p orbitals with an occupation of 1.99. The orbitals with an occupation of 1.00 have significant amounts of f character only and essentially correspond to a $5f^3$ electronic configuration per U atom as the dominant electronic configuration. A natural orbital is also present below the HOMO−LUMO region, showing bonding interaction between uranium and the bridging hydrides (Figure 7); however, there is less delocalization of the electron density of this actinide−hydride bond compared to that of **1**. Similarly to its tetravalent analogue, **2** is a single electronic configuration, 4U $6p^2$ 2U $5f^3$, with a weighting of 0.98.

1/2 Interconversion. The interconversion energies of the tetravalent and trivalent actinide hydride complexes (Scheme 3) were calculated at the PBE/def-TZVP and CASPT2/ANO-RCC-VDZP levels. The energy to interconvert **1** to produce **2** + H_2 was predicted to be thermoneutral at 0.3 kcal/mol at the CASPT2 level, based on just the electronic energies. Including the zero-point energy calculated at the PBE level [ΔH_{rxn}(ZPE) = −2.44 kcal/mol] results in an exothermic reaction at −2.2 kcal/mol. On the basis of the thermodynamics, **1** readily releases molecular H_2 in an

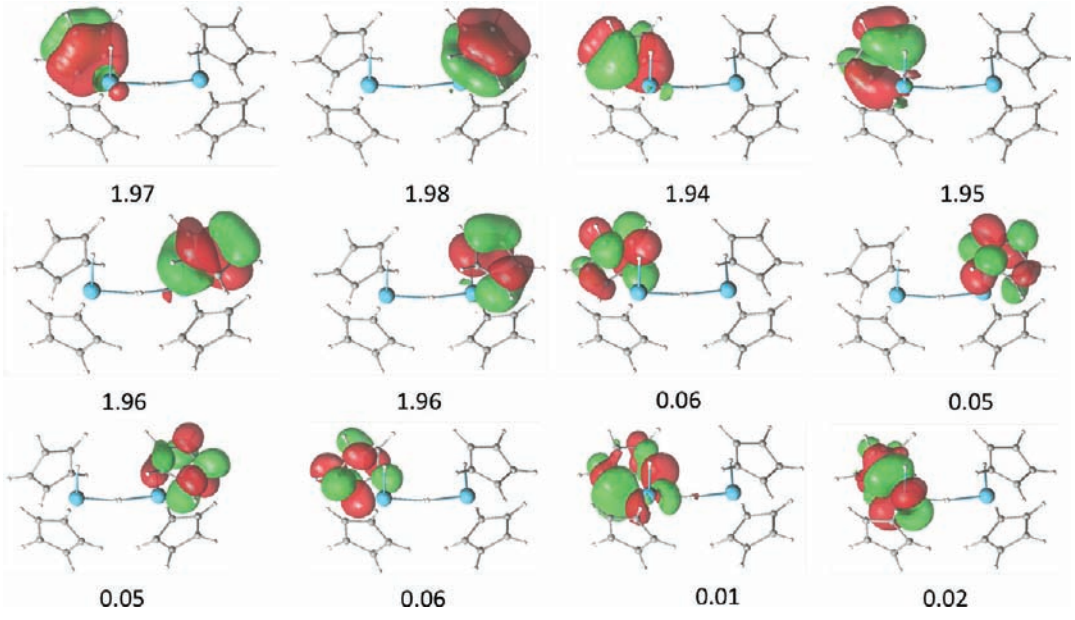

Figure 3. Molecular orbitals responsible for the bonding in $[(C_5H_5)_2ThH_2]_2$ (singlet) for a (12, 12) active space. Respective occupation numbers are indicated below the orbital plots (isovalue 0.04). Color code: Th, blue; C, gray; H, white.

dx.doi.org/10.1021/ic202503h | *Inorg. Chem.* 2012, 51, 3613−3624

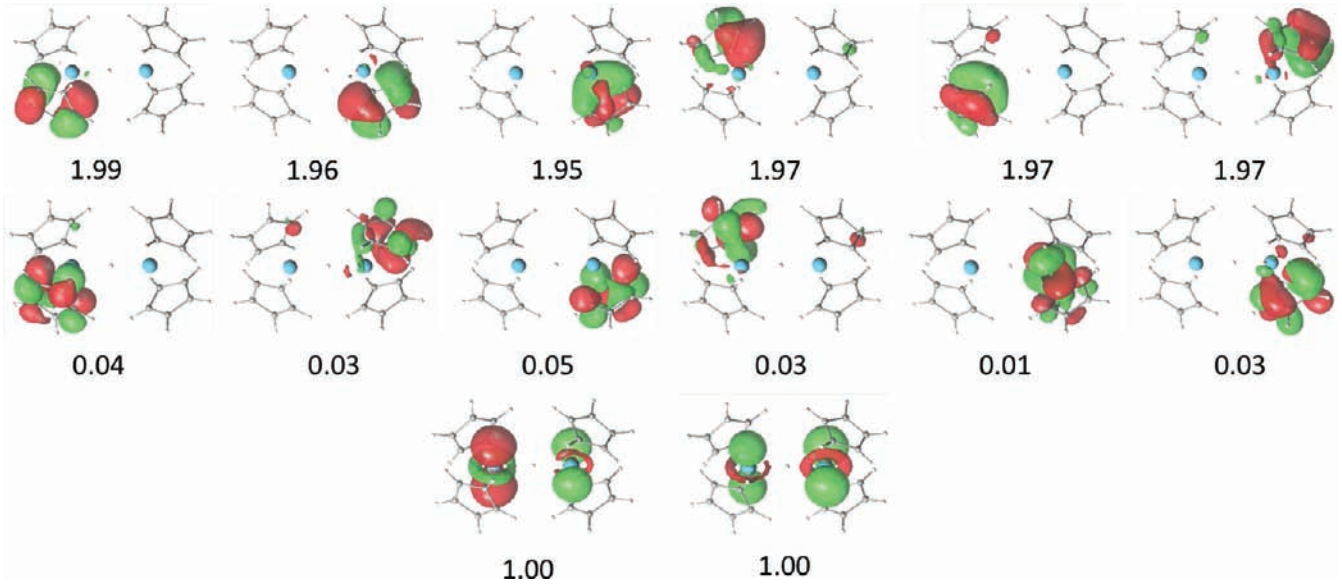

Figure 4. Molecular orbitals responsible for the bonding in $[(C_5H_5)_2ThH]_2$ (triplet) with a (14, 14) active space. Respective occupation numbers are indicated below the orbital plots (isovalue 0.04). Color code: Th, blue; C, gray; H, white.

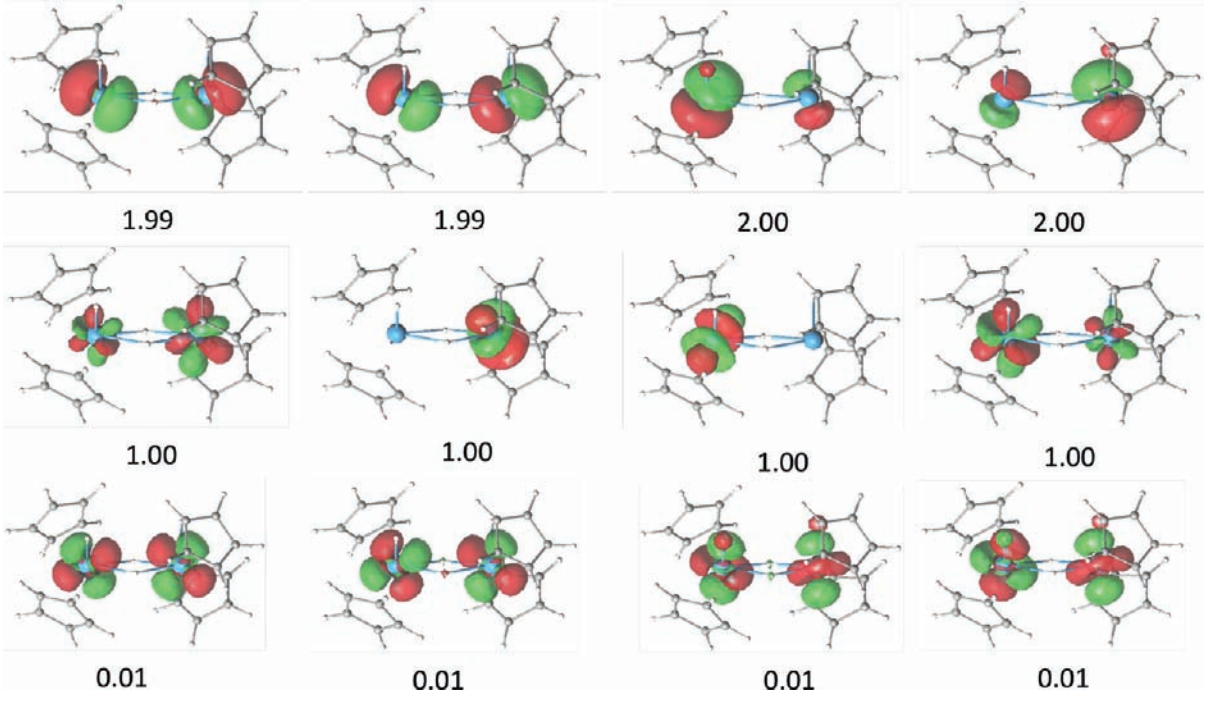

Figure 5. Molecular orbitals responsible for the bonding in $[(C_5H_5)_2UH_2]_2$ (quintet) with a (12, 12) active space. Respective occupation numbers are indicated below the orbital plots (isovalue 0.04). Color code: U, blue; C, gray; H, white.

exothermic process to form **2** in a reaction that is possibly a formal bimetallic reductive elimination. At the PBE level, the equivalent reaction was predicted to be endothermic by 4.6 kcal/mol at the electronic energy level, which decreases to 2.2 kcal/mol upon inclusion of ΔH_{rxn}(ZPE). The PBE result is in reasonable agreement with the CASPT2 value. The interconversion energy is marginally exothermic based on the CASPT2 result. This is consistent with the spontaneous release of H_2 from isolated samples of **1** and the formation of an equilbrium mixture of **1** and **2**.[2]

In contrast to the uranium system, the interconversion of **3** to produce **4** + H_2 is substantially endothermic by 27.6 kcal/mol at the CASPT2 level and 35.9 kcal/mol at the PBE level, based on the electronic energies. The endothermicity decreases to 25.7 and 34.0 kcal/mol, respectively, when ΔH_{rxn}(ZPE) (1.93 kcal/mol) is included. Unlike the uranium system, the interconversion of the tetravalent and trivalent thorium hydride complexes is largely endothermic. This is consistent with the difficulty in isolating thorium(3+) complexes,[4−7] and a sizable HOMO−LUMO gap of **3** (2.70 eV) and a marginal gap found in **4** of 0.53 eV, which contrasts that of the uranium(4+) (**1**)−uranium(3+) (**2**) complexes with more comparable gaps of 2.43 versus 2.89 eV (Table 3), respectively. Both CASPT2 and DFT are in good agreement in predicting interconversion ener-

dx.doi.org/10.1021/ic202503h | *Inorg. Chem.* 2012, 51, 3613−3624

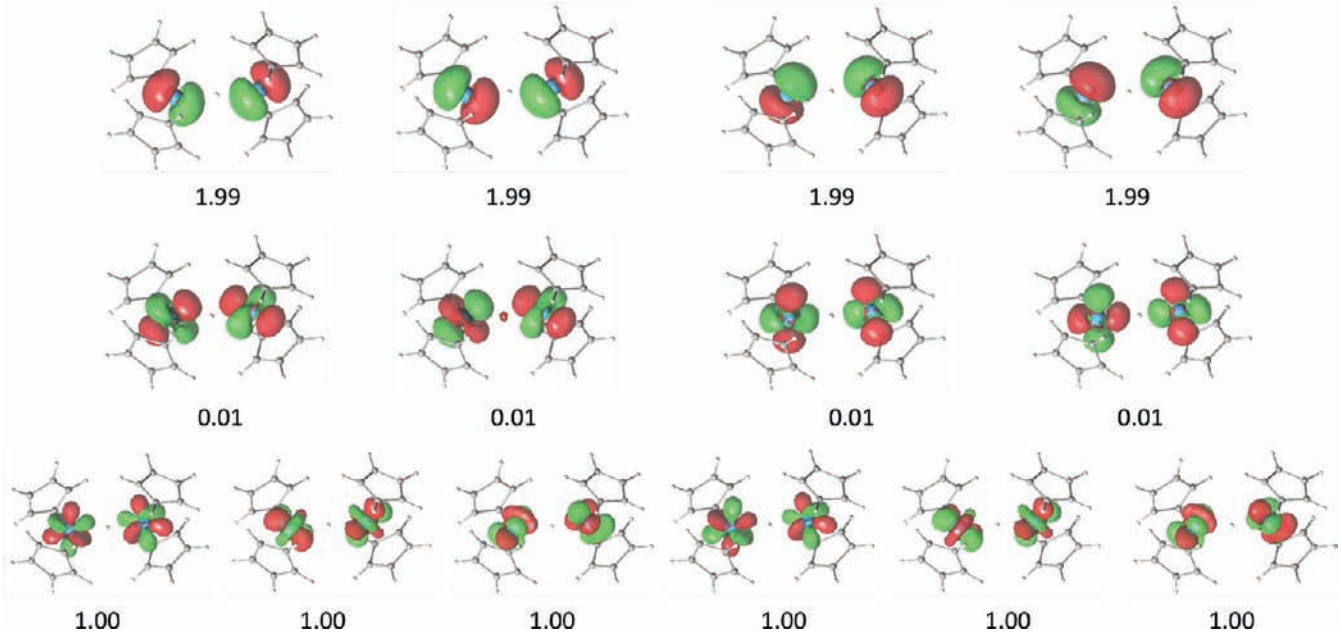

Figure 6. Molecular orbitals responsible for the bonding in $[(C_5H_5)_2UH]_2$ (septet) with a (14, 14) active space. Respective occupation numbers are indicated below the orbital plots (isovalue 0.04). Color code: U, blue; C, gray; H, white.

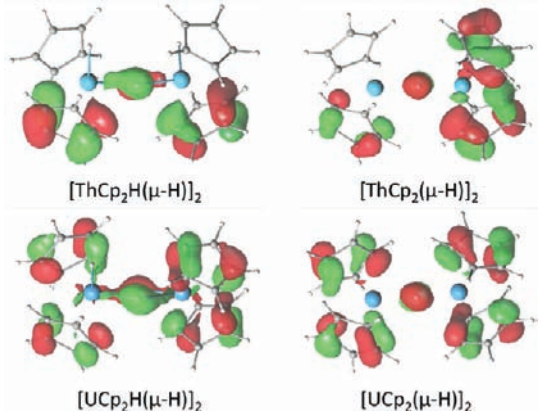

Figure 7. Molecular orbital illustrating a bonding interaction between the actinide metal and bridging hydrides. The occupation numbers are all 2.00 (isovalue 0.04). Color code: Th and U, blue; C, gray; H, white.

Scheme 3

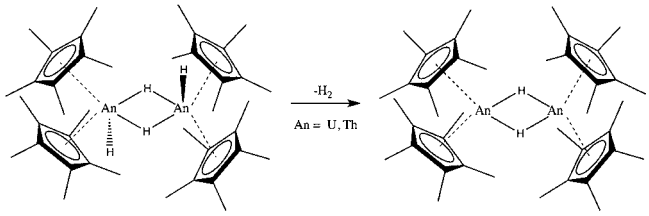

gies given that each method predicts the same ground state for each species to within 1 kcal/mol, although there was larger disagreement with the relative state energies.

DISCUSSION

Actinide hydrides represent a combination of extremes in the periodic table involving bonds between the element with the smallest atomic number and the heaviest elements available, in turn, making experimental analysis by commonly used techniques rather difficult. X-ray crystallography cannot accurately locate the one-electron H atoms in the presence of the 92-electron U atoms. Similarly, NMR spectroscopy is not able to locate hydrogen in the presence of the paramagnetic metal. Even IR spectroscopy in the complexes described here is not very informative because the observed absorptions are very broad and do not indicate that two types of hydrides are present. One of the specific complexes examined in this study, **1**, presents an additional challenge in that it readily loses H_2 at room temperature. It needs to be handled under H_2 pressure to retain its integrity, and in some cases, it can rupture glass vessels in which it is sealed because of H_2 buildup.

With such experimental difficulties, it is highly desirable to be able to predict the structure, properties, and reactivity theoretically. However, from a theoretical standpoint, such an analysis is also challenging. The comparable energies of crystal-field splitting and spin−orbit coupling for these heavy metals do not allow simple models of analysis to be used, and the need to consider relativistic effects also adds to the challenge. In addition, the open-shell nature of the U^{4+} $5f^2$ and U^{3+} $5f^3$ complexes makes theoretical calculations on these compounds more difficult, often requiring the use of multiconfigurational (CASSCF/CASPT2) methods for accurate analyses. Given all of these difficulties, relatively few theoretical and experimental studies are undertaken on this fundamental type of actinide complex even with the simplest ligands available.

One of the main goals in this study was to determine whether theory could provide useful insight into these challenging systems. The specific actinide hydrides examined, **1**−**4**, were chosen for several reasons. Pairing the U^{4+} $5f^2$ complex **1** and the Th^{4+} $5f^0$ complex **3** provides an open-shell and closed-shell analogue comparison, respectively, while examining the uranium(3+) complex **2** and the thorium(3+) complex **4** allows a comparison of a known and an experimentally unknown compound. Complex **4** also provides the opportunity to look at a single electron valence configuration that could be either $5f^1$ or $6d^1$. In addition, the fact that there is a reversible reductive elimination and oxidative addition reaction occurring between

dx.doi.org/10.1021/ic202503h | Inorg. Chem. 2012, 51, 3613−3624

1 and 2 and an analogous reaction has not been observed for the Th^{4+}/Th^{3+} pair, 3 and 4, provides an experimental framework upon which to validate theory in predicting the reactivity in these actinide hydrides. An additional advantage of these complexes is that large crystals of 1 could be isolated so that neutron diffraction data are available not only for 3 but also for its uranium analogue.

Neutron diffraction analysis of 1 demonstrated successful data collection even with a highly reactive species that decomposes unless under H_2 pressure. The structural information obtained on 1 from the two neutron diffraction data sets and the two X-ray diffraction experiments shows an overall confluence in the structure. However, these data sets demonstrate that even for the U···U distances variations as large as 0.08 Å can occur depending on the data collection method and temperature.

Overall, the calculations illustrate good agreement with the experimental structural data on 1−3. Hence, the calculations on the An−C, C−C, and C−H distances and the (C_5Me_5 ring centroid)−An−(C_5Me_5 ring centroid) angles all match the experimental data well. The An−H distances also match the experimental values quite well, although these have larger error limits. This is another case in which theory can provide information not obtainable by experiment. The An···An nonbonding distance predictions are close for 2 and 3, but the calculations do not match this parameter as well for 1, even though this parameter also shows considerable experimental variation. The reasons for this are unclear. Hence, both experimental and theoretical data on such distances must not be overinterpreted.

For the tetravalent and trivalent thorium hydride complexes, the natural orbital plots obtained at the CASPT2/ANO-RCC-VDZP level indicate that the orbitals in the HOMO−LUMO region essentially correspond to bonding and antibonding orbitals on the cyclopentadienyl ligands. In contrast, the natural orbitals of the tetravalent and trivalent uranium hydride complexes are mainly localized on uranium as opposed to the cyclopentadienyl ligands. This suggests an important distinction between thorium and uranium. Localization of the HOMO electron density on the ligands in the thorium complexes may give them more free-ligand-like reactivity than the uranium complexes. In addition, bonding orbitals between the actinide metals and the bridging H atoms were observed just below the HOMO−LUMO regions in each case.

Finally, the calculations also match well the observed interconversion of 1 and 2, and the fact that 3 does not form 4 analogously. Hence, the energies of 1 and 2 are found to be similar, and 3 is much more stable than 4. The successful results of this test case suggest that theory at this level can be adequately used to evaluate the viability of such unknown species.

CONCLUSIONS

DFT (PBE/def-TZVP) and multiconfigurational CASPT2/ANO-RCC-VDZP calculations have been performed on the tetravalent and trivalent actinide hydride complexes of thorium and uranium, specifically 1−4. Geometries calculated at the PBE/def-TZVP level are in good agreement with the available X-ray and neutron diffraction data. Natural orbital analyses of the thorium hydride complexes indicate orbital localization in the HOMO−LUMO region to the cyclopentadienyl ligands, in contrast to the analogous uranium hydrides, mainly showing localization on uranium. A bonding orbital between the actinide metal and bridging H atoms was observed just below the HOMO−LUMO region. The energy to convert 1 to 2 + H_2 was predicted to be near thermoneutral (∼−2 kcal/mol) and substantially less endothermic than the analogous thorium reaction of 26 kcal/mol.

ASSOCIATED CONTENT

Supporting Information

xyz coordinates of the optimized DFT structures as well as crystallographic data on 1. This material is available free of charge via the Internet at http://pubs.acs.org.

AUTHOR INFORMATION

Corresponding Author

*E-mail: gagliard@umn.edu (L.G.), wevans@uci.edu (W.J.E.).

Present Address

[‖]Australian Nuclear Science and Technology Organisation, Lucas Heights, New South Wales 2234, Australia.

Notes

The authors declare no competing financial interest.

ACKNOWLEDGMENTS

This work was supported by the Director, Office of Basic Energy Sciences, U.S. Department of Energy, under Contract USDOE/DE-SC002183, the University of Minnesota Supercomputing Institute, and the Chemical Sciences, Geosciences, and Biosciences Division of the Office of Basic Energy Sciences of the Department of Energy under Grant DE-FG02-10ER16161. We also thank Jorg Meyer for flame-sealing the samples under H_2 and Dr. Ming Fang for assistance.

REFERENCES

(1) Marks, T. J.; Fagan, P. J.; Manriquez, J. M.; Maatta, E. A.; Seyam, A. M. *J. Am. Chem. Soc.* **1981**, *103*, 6650−6667.

(2) Evans, W. J.; Miller, K. A.; Kozimor, S. A.; Ziller, J. W.; DiPasquale, A. G.; Rheingold, A. L. *Organometallics* **2007**, *26*, 3568−3576.

(3) Broach, R. W.; Schultz, A. J.; Williams, J. W.; Brown, G. M.; Manriquez, J. M.; Fagan, P. J.; Marks, T. J. *Science* **1979**, *203*, 172−174.

(4) Blake, P. C.; Lappert, M. F.; Atwood, J. L.; Zhang, H. *J. Chem. Soc., Chem. Commun.* **1986**, 1148−1149.

(5) Parry, J. S.; Cloke, F. G. N.; Coles, S. J.; Hursthouse, M. B. *J. Am. Chem. Soc.* **1999**, *121*, 6867−6871.

(6) Blake, P. C.; Edelstein, N. M.; Hitchcock, P. B.; Kot, W. K.; Lappert, M. F.; Shalimoff, G. V.; Tian, S. *J. Organomet. Chem.* **2001**, *636*, 124−129.

(7) Walensky, J. R.; Martin, R. L.; Ziller, J. W.; Evans, W. J. *Inorg. Chem.* **2010**, *49*, 10007−10012.

(8) For more information on drying systems, see www.glasscontour.com.

(9) Keen, D. A.; Gutmann, M. J.; Wilson, C. C. *J. Appl. Crystallogr.* **2006**, *39*, 714−722.

(10) For more information, see http://www.ill.eu/instruments-support/instruments groups/instruments/d19/characteristics/.

(11) Wilkinson, C.; Khamis, H. W.; Stansfield, R. F.; McIntyre, G. J. *J. Appl. Crystallogr.* **1988**, *21*, 471−478.

(12) Hohenberg, P.; Kohn, W. *Phys. Rev.* **1964**, *136*, 864−871.

(13) Kohn, W.; Sham, L. J. *Phys. Rev.* **1965**, *140*, 1133−1138.

(14) Roos, B. O.; Taylor, P. R.; Siegbahn, P. E. M. *Chem. Phys.* **1980**, *48*, 157−173.

(15) Andersson, K.; Malmqvist, P.-Å.; Roos, B. O. *J. Chem. Phys.* **1992**, *96*, 1218.

(16) Perdew, J. P.; Burke, K.; Ernzerhof, M. *Phys. Rev. Lett.* **1996**, *77*, 3865−3868.

(17) Schaefer, A.; Huber, C.; Ahlrichs, R. *J. Chem. Phys.* **1994**, *100*, 5829. Eichkorn, K.; Weigend, F.; Treutler, O.; Ahlrichs, R. *Theor. Chem. Acc.* **1997**, *97*, 119−124.
(18) Cao, X. Y.; Dolg, M. *J. Chem. Phys.* **2001**, *115*, 7348.
(19) Ahlrichs, R.; Bar, M.; Haser, M.; Horn, H.; Kolmel, C. *Chem. Phys. Lett.* **1989**, *162*, 165−169.
(20) Hess, B. A. *Phys. Rev. A* **1986**, *33*, 3742−3748.
(21) Roos, B. O.; Lindh, R.; Malmqvist, P.-Å.; Veryazov, V.; Widmark, P. O. *J. Phys. Chem. A* **2005**, *109*, 6575−6579.
(22) Karlström, G.; Lindh, R.; Malmqvist, P.-Å.; Roos, B. O.; Ryde, U.; Veryazov, V.; Widmark, P.-O.; Cossi, M.; Schimmelpfennig, B.; Neogrady, P.; Seijo, L. *Comput. Mater. Sci.* **2003**, *287*, 222−239.
(23) Aquilante, F.; Gagliardi, L.; Pedersen, T. B.; Lindh, R. *J. Chem. Phys.* **2009**, *130*, 154107.
(24) Aquilante, F.; Pedersen, T. B.; Lindh, R.; Roos, B. O.; De Meras, A. S.; Koch, H. *J. Chem. Phys.* **2008**, *129*, 024113.
(25) Aquilante, F.; Malmqvist, P. A.; Pedersen, T. B.; Ghosh, A.; Roos, B. O. *J. Chem. Theory Comput.* **2008**, *4*, 694−702.
(26) Aquilante, F.; Pedersen, T. B.; Lindh, R. *J. Chem. Phys.* **2007**, *126*, 194106.
(27) Gagliardi, L.; Roos, B. O. *Chem. Soc. Rev.* **2007**, *36*, 893−903. Gagliardi, L. *J. Am. Chem. Soc.* **2003**, *125*, 7504−7505.
(28) La Macchia, G.; Brynda, M.; Gagliardi, L. *Angew. Chem., Int. Ed.* **2006**, *45*, 6210−6213.
(29) Gagliardi, L.; Heaven, M. C.; Krogh, J. W.; Roos, B. O. *J. Am. Chem. Soc.* **2005**, *127*, 86−91.
(30) Gagliardi, L.; La Manna, G.; Roos, B. O. *Faraday Discuss.* **2003**, *124*, 63−68.
(31) Fendrick, C. M.; Schertz, L. D.; Day, V. W.; Marks, T. J. *Organometallics* **1988**, *7*, 1828−1838.
(32) Shannon, R. D. *Acta Crystallogr., Sect. A* **1976**, *32*, 751−767.